





Quadratic phase mismatch in multisoliton interferograms based on time-stretched dispersive Fourier transformation

Zeqing Li ^{1,2,3,*} Benhai Wang ^{2,3,4,*} Wenbin He ^{2,4,†} Qi Huang^{2,3,4} Xiaocong Wang,^{1,2,5}
Xintong Zhang,^{1,2,5} and Meng Pang ^{1,2,4,‡}

¹*State Key Laboratory of High Field Laser Physics and CAS Center for Excellence in Ultra-intense Laser Science, Shanghai Institute of Optics and Fine Mechanics, Chinese Academy of Sciences, Shanghai 201800, China*

²*Russell Centre for Advanced Lightwave Science, Shanghai Institute of Optics and Fine Mechanics and Hangzhou Institute of Optics and Fine Mechanics, Hangzhou, Zhejiang 311421, China*

³*Center of Materials Science and Optoelectronics Engineering, University of Chinese Academy of Sciences, Beijing 100049, China*

⁴*Innovation and Integration Center of New Laser Technology, Shanghai Institute of Optics and Fine Mechanics, Chinese Academy of Sciences, Shanghai 201800, China*

⁵*Department of Optics and Optical Engineering, University of Science and Technology of China, Hefei, Anhui 230026, China*



(Received 1 February 2024; accepted 6 May 2024; published 20 May 2024)

The time-stretched dispersive Fourier transform method (TS-DFT) has been widely used to analyze multisoliton structures in ultrafast lasers, featuring shot-by-shot access to their spectral interferograms. Most exemplary structures consist of two interacting solitons whose spacing and relative phase can be simply retrieved from their interferograms mapped in time domain by TS-DFT. However, such analysis has not been elaborated for structures with more solitons that could result in a complicated TS-DFT signal. Here we report our theoretical inference of a deterministic discrepancy when retrieving structures consisting of more than two solitons with their TS-DFT signal. We unveil the underlying source of these discrepancies as a result of the quadratic phase mismatch induced by TS-DFT and correspondingly propose an improved retrieval method. Our work may provide a theoretical guideline for conducting unambiguous analysis of complex multipulse structures using TS-DFT, particularly when the dispersive stretching ratio is limited.

DOI: [10.1103/PhysRevA.109.053524](https://doi.org/10.1103/PhysRevA.109.053524)

I. INTRODUCTION

Multisoliton structures are ubiquitous in ultrafast lasers and are epitomized by the so-called soliton molecules, which feature compact structures that stem from direct interactions between the particlelike optical solitons and host a series of inspiring light-matter analogies [1–4] and nonbinary encoding possibilities [5], therefore attracting interdisciplinary interest. The dissipative nature of ultrafast lasers often makes the interaction mechanism between optical solitons highly complicated [6–8]. Nevertheless, the key parameters that indicate the strength and direction of the interactions are simply the spacing and relative phase of the interacting solitons, particularly when they interact directly through partial overlapping [9,10], which can be controlled in different ways [5,11,12].

In practice, the dynamics of multisoliton structures have been routinely analyzed using the time-stretched dispersive Fourier transform (TS-DFT) method [13–15], which can provide direct time-frequency mapping for ultrafast laser fields. Using dispersive temporal stretching, the TS-DFT method enables shot-by-shot access to the spectral interferograms of multisoliton structures mapped in the time domain, from

which the spacing and relative phase between the solitons can be retrieved simultaneously [2,3]. Previous reported studies on multisoliton dynamics in ultrafast lasers mainly focused on double-soliton structures [2,3] which produce simple interferograms that can be linearly mapped in the time domain by TS-DFT. The evolving soliton spacing and relative phase can then be readily retrieved shot by shot from the period and relative offset of the interferometric fringe beneath the spectral envelope [16].

Recently, complex multisoliton structures in ultrafast lasers that involve a greater number of solitons, e.g., triple-soliton molecules [16–20] or beyond [21–25], have attract wide interest due to the rich dynamics of collective soliton interactions and extended flexibility in the manipulation of ultrafast laser fields. However, the precise retrieval of these structures directly from their TS-DFT signal becomes challenging due to the fact that structures consisting of more than two solitons would result in complex interferograms with multiple interleaved interferometric fringes beneath the spectral envelope, leading to potential ambiguities during the retrieving procedure. Here we report a theoretical finding that the TS-DFT signal of triple-soliton structures (or even a greater number of solitons) is actually not a linear mapping of their genuine spectral interferograms, even when the stationary phase approximation [14,26] has been incorporated. We unveil that the quadratic phase profile induced by the dispersive stretching could cause phase mismatch between each pair

*These two authors contributed equally to this work.

†wenbin.he@r-cals.com

‡pangmeng@siom.ac.cn

of solitons in these structures and, eventually, lead to deterministic discrepancies when retrieving the relative phases between these solitons. Such discrepancies become prominent especially when the stretching ratio is limited when using the TS-DFT method. Both analytical and numerical analyses are performed to clearly identify the cause and extent of this discrepancy. Based on this analysis, we also propose an improved retrieval method that can eliminate the quadratic phase mismatch.

II. THEORETICAL ANALYSIS

A. The quadratic phase term induced by TS-DFT

Using the TS-DFT method, the spectral profile of ultrafast pulses can be mapped in the time domain provided there is sufficient temporal stretching in a length of dispersive fiber [26]. The linear pulse propagation in an optical fiber with group velocity dispersion β_2 is governed by

$$\frac{\partial U(\zeta, \tau)}{\partial \zeta} + \frac{i}{2} \text{sgn}(\beta_2) \frac{\partial^2 U(\zeta, \tau)}{\partial \tau^2} = 0, \quad (1)$$

in which $U(\zeta, \tau)$ is the normalized pulse profile that gives a unit peak power, $\zeta = z/L_D$ gives a normalized propagation distance, where L_D is the dispersion length defined as $L_D = T_0^2/|\beta_2|$, and $\tau = T/T_0$ gives a normalized time in a moving frame, with T_0 the pulse duration. The analytic form of $U(\zeta, \tau)$ can be obtained as

$$U(\zeta, \tau) = \frac{1}{2\pi} \int_{-\infty}^{\infty} \tilde{U}(0, \tilde{\omega}) \exp\left[\frac{i}{2} \text{sgn}(\beta_2) \zeta \tilde{\omega}^2 - i\tilde{\omega}\tau\right] d\tilde{\omega}, \quad (2)$$

where $\tilde{U}(0, \tilde{\omega})$ is the complex amplitude spectrum of $U(0, \tau)$. Here we use normalized angular frequency $\tilde{\omega}$ defined as $\tilde{\omega} = T_0(\omega - \omega_0)$, where ω_0 is the carrier frequency of the pulse. Given large enough ζ that entails a stationary phase approximation [26], the resultant pulse envelope can be obtained assuming that the integral term in Eq. (2) is valuable only at $\tilde{\omega} = \tau/[\text{sgn}(\beta_2)\zeta]$, which gives

$$U(\zeta, \tau) = \frac{\exp\left[-i \text{sgn}(\beta_2) \frac{\tau^2}{2\zeta}\right]}{[1 - i \text{sgn}(\beta_2)]\sqrt{\pi\zeta}} \tilde{U}\left[0, \text{sgn}(\beta_2) \frac{\tau}{\zeta}\right]. \quad (3)$$

Thus, it can be seen from Eq. (3) that the time-domain waveform will be monotonically broadened to its frequency spectrum $\tilde{U}(0, \tilde{\omega})$ with a linear mapping of frequency in the time domain as

$$\tilde{\omega} = \text{sgn}(\beta_2) \frac{\tau}{\zeta}. \quad (4)$$

We can notice that there is a complex phase term $\exp[-i \text{sgn}(\beta_2) \tau^2/2\zeta]$ in Eq. (3) with a quadratic relation with τ (quadratic phase) in addition to the complex amplitude spectrum $\tilde{U}(0, \tilde{\omega})$. When the intensity field is detected (e.g., using a fast photodetector), this quadratic phase will disappear, leading to a simple intensity signal which is directly proportional to the intensity spectrum profile, i.e.,

$$|U(\zeta, \tau)|^2 = \frac{1}{2\pi\zeta} \left| \tilde{U}\left[0, \text{sgn}(\beta_2) \frac{\tau}{\zeta}\right] \right|^2. \quad (5)$$

It is critical to emphasize that the stationary phase approximation used in the derivation from Eq. (2) to Eq. (4) is valid only if the imaginary part of $\tilde{U}(0, \tilde{\omega})$ is $\tilde{\omega}$ independent. As a result, for a single pulse profile without any chirp in the carrier phase, the TS-DFT signal [Eq. (5)] and its spectral interferogram conform to a linear mapping relationship given by Eq. (4), with the linear relationship sharing the same temporal origin with the pulse profile $U(0, \tau)$. However, for two or more pulse structures, the spacing between the pulses brings a $\tilde{\omega}$ -dependent linear phase shift to $\tilde{U}(0, \tilde{\omega})$, thus making the stationary phase approximation condition invalid for the above derivations. Consequently, the TS-DFT signal is no longer a linear mapping of its genuine spectral interferogram. This is the underlying reason for the complication of the multipulse TS-DFT signal, as we will derive in detail below. Therefore, in the following derivations, we apply the stationary phase approximation as a valid assumption only for each single pulse when considering the TS-DFT signal for two- or more-pulse structures, and consequent discrepancy between the temporal and spectral interferograms can then be derived as a result of the multipulse structure.

B. Multisoliton interferograms by TS-DFT

1. The case with double-soliton structure

In a double-soliton structure, the temporal profile of each individual soliton U_j can be written as

$$U_j(0, \tau) = U(0, \tau - \tau_j) \exp(-i\varphi_j), \quad j = 0, 1, \quad (6)$$

where $U(0, \tau)$ represents a soliton profile at origin with null carrier phase, whose Fourier transform is $\tilde{U}(0, \tilde{\omega})$, while τ_j and φ_j are the temporal position and carrier phase of two pulses in the normalized time coordinate. The corresponding spectral interferogram $|\tilde{U}_m|^2$ of the double-pulse structure $U_m = \sum_j U_j$ can then be obtained as

$$|\tilde{U}_m(0, \tilde{\omega})|^2 = |\tilde{U}(0, \tilde{\omega})|^2 [2 + \cos(\Delta\tau_{10}\tilde{\omega} - \Delta\varphi_{10})], \quad (7)$$

where $\Delta\tau_{10} = \tau_1 - \tau_0$ and $\Delta\varphi_{10} = \varphi_1 - \varphi_0$. Here the spectral envelope and the interferometric fringe shared the same frequency coordinate, both referring to zero normalized frequency (or at the carrier frequency). However, when mapping this interferogram in the time domain, the envelope and the interferometric fringe of the TS-DFT signal do not necessarily share the same temporal coordinate (i.e., with temporal offset between each other), as we will derive below.

The complex amplitude of the TS-DFT signal of each individual pulse can be written as [see Eq. (3)]

$$U_j(\zeta, \tau) = \frac{\exp(i\Phi_j)}{(1+i)\sqrt{\pi\zeta}} \tilde{U}\left(0, -\frac{\tau - \tau_j}{\zeta}\right), \quad j = 0, 1. \quad (8)$$

Here we assume $\text{sgn}(\beta_2) = -1$ for simplicity since we mostly use the standard SMF-28 optical fiber, which has anomalous dispersion for the TS-DFT method. The quadratic phase term Φ_j can be expressed as

$$\begin{aligned} \Phi_j &= \frac{(\tau - \tau_j)^2}{2\zeta} - \varphi_j \\ &= \frac{\tau^2}{2\zeta} - \tau_j \left(\frac{\tau - \frac{1}{2}\tau_j}{\zeta} \right) - \varphi_j, \quad j = 0, 1. \end{aligned} \quad (9)$$

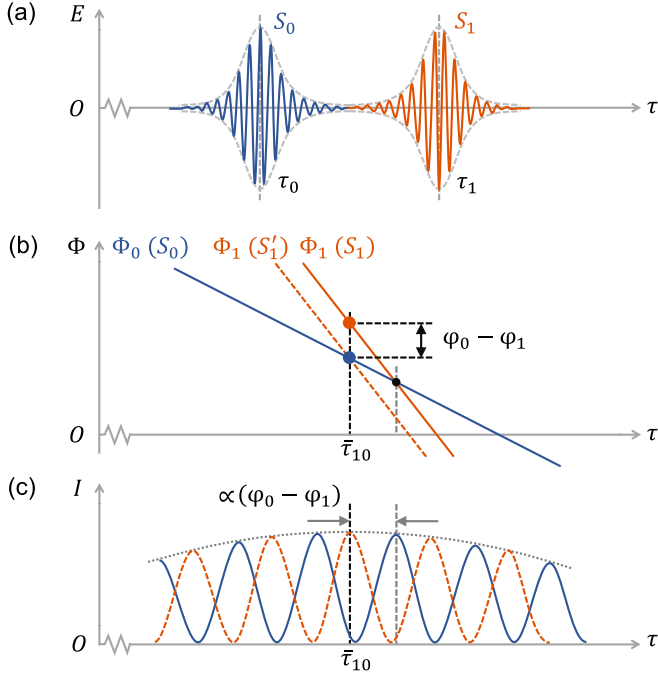


FIG. 1. Double-soliton TS-DFT signal schematic. (a) A double-soliton structure in the normalized time coordinate. The gray dashed line gives the envelope profile. The two solitons are denoted as S_0, S_1 , with their temporal positions at τ_0 and τ_1 , respectively. (b) The linear part of the quadratic phase Φ_j , $j = 0, 1$ [second plus third terms in Eq. (9)]. S'_1 denotes the special case when $\varphi_1 = \varphi_0$ such that linear parts of Φ_0 and Φ_1 intersect at $\bar{\tau}_{10}$. In general, the phase difference between S_0 and S_1 can be obtained at $\bar{\tau}_{10}$ as the vertical distance between the two lines. (c) The TS-DFT signal of the double-soliton structure. The orange dashed curve gives the sinusoidal fringes when $\Delta\varphi_{10} = 0$. Given $\Delta\varphi_{10} \neq 0$, the sinusoidal fringe shifts correspondingly beneath the envelope (the gray dashed line), which is given by the solid blue curve.

The first quadratic term $\tau^2/2\zeta$ is the same for every pulse; thus it plays no role in the TS-DFT signal that only concerns the difference between these quadratic phase terms. The second term represents a linearly changing phase difference across the envelope profile, while the third term (the intrinsic carrier phase) adds an offset upon it. These last two terms determine the exact period and offset of the sinusoidal fringe in the result [Figs. 1(b) and 1(c)]. After sufficient dispersive stretching, the envelope width of the two pulses becomes much larger than the initial pulses' spacing and approximately merges at the middle point of the two pulses, $\bar{\tau}_{10} = (\tau_1 + \tau_0)/2$, which can be regarded as the center of the TS-DFT signal envelope. The power of the TS-DFT signal of a double-soliton structure can be expressed as

$$|U_m(\zeta, \tau)|^2 = \frac{1}{2\pi\zeta} \left| \tilde{U}\left(0, -\frac{\tau - \bar{\tau}_{10}}{\zeta}\right) \right|^2 [2 + \cos(\Phi_1 - \Phi_0)], \quad (10)$$

where we replace both τ_0 and τ_1 of each soliton envelope with $\bar{\tau}_{10}$ due to the sufficient stretching. The phase difference $\Phi_1 - \Phi_0$ between the two time-stretched envelopes can be

expressed as

$$\Phi_1 - \Phi_0 = -\Delta\tau_{10} \frac{\tau - \bar{\tau}_{10}}{\zeta} - \Delta\varphi_{10}. \quad (11)$$

By comparing Eqs. (10) and (7), we can notice that the TS-DFT signal and spectral interferogram satisfy a linear mapping relation, i.e.,

$$\tilde{\omega}_{\text{double}} = -\frac{\tau - \bar{\tau}_{10}}{\zeta}, \quad (12)$$

which differs from Eq. (4) only by a temporal shift $\bar{\tau}_{10}$ (the middle point of the double-soliton structure). Here we put a subscript to $\tilde{\omega}$ to emphasize that such mapping relation is valid only for a double-soliton structure. Using $\bar{\tau}_{10}$ as the reference point for analyzing the phase difference between pulses, $\Delta\varphi_{10}$ can be retrieved without discrepancy.

2. The case with triple-soliton structures

Given more than two solitons in the structure, the TS-DFT signal features multiple interleaved sinusoidal fringes that lead to an intricate profile. Importantly, similar to the case in the double-soliton case, we unveiled that the envelope and each sinusoidal fringe in the TS-DFT signal actually refer to different origins in the temporal coordinate due to the phase mismatch. Such mismatch can no longer be removed by a simple temporal offset and will eventually cause discrepancies when still retrieving the relative phase by the form of its spectral interferogram, as will be illustrated below.

The spectral interferogram of a triple-soliton structure can be expressed as

$$|\tilde{U}_m(0, \tilde{\omega})|^2 = |\tilde{U}(0, \tilde{\omega})|^2 \left[3 + 2 \sum_{j=1}^2 \sum_{k=0}^{j-1} \cos(\Delta\tau_{jk}\tilde{\omega} - \Delta\varphi_{jk}) \right], \quad (13)$$

where the interferometric fringes consist of three different sinusoidal modulations, each corresponding to one pair of solitons among the three solitons. The TS-DFT signal of the triple-soliton structure, on the other hand, can be expressed as

$$U_m(\zeta, \tau) = \sum_{j=0}^2 \frac{\exp(i\Phi_j)}{(1+i)\sqrt{\pi\zeta}} \tilde{U}\left(0, -\frac{\tau - \tau_j}{\zeta}\right), \quad (14)$$

where Φ_j satisfies Eq. (9). Similar to the case with a double soliton, the stretched envelope centers approximately at the averaged position of all three solitons, i.e.,

$$\bar{\tau} = \frac{1}{3} \sum_{j=0}^2 \tau_j. \quad (15)$$

Then, we can rewrite Eq. (14) as

$$|U_m(\zeta, \tau)|^2 \approx \frac{1}{2\pi\zeta} \left| \tilde{U}\left(0, -\frac{\tau - \bar{\tau}}{\zeta}\right) \right|^2 \times \left[3 + 2 \sum_{j=1}^2 \sum_{k=0}^{j-1} \cos(\Phi_j - \Phi_k) \right], \quad (16)$$

where the phase difference term $\Phi_k - \Phi_j$, similar to the case in Eq. (11), can be expressed as

$$\Phi_j - \Phi_k = -\Delta\tau_{jk} \frac{\tau - \bar{\tau}_{jk}}{\zeta} - \Delta\varphi_{jk}, \quad (17)$$

in which

$$\bar{\tau}_{jk} = \frac{\tau_j + \tau_k}{2}. \quad (18)$$

By comparing Eqs. (13) and (16), we can find out that the signal envelope \tilde{U} has a mapped frequency $\tilde{\omega}_{\text{envelope}}$ in the time domain expressed as

$$\tilde{\omega}_{\text{envelope}} = -\frac{\tau - \bar{\tau}}{\zeta}, \quad (19)$$

while the sinusoidal fringe generated by each pair of solitons (with the middle point position at $\bar{\tau}_{jk}$) has its own mapping relation with a different offset,

$$\tilde{\omega}_{jk} = -\frac{\tau - \bar{\tau}_{jk}}{\zeta}. \quad (20)$$

Here, $\tilde{\omega}_{jk}$ denotes the mapped frequency for the sinusoidal fringe produced by solitons j and k . Therefore, although the envelope and fringes of the TS-DFT signal share the same magnification ratio in a linear mapping relationship, they have different temporal offsets due to the mismatch between the averaged position of all pulses, $\bar{\tau}$, and each pair of pulses, $\bar{\tau}_{jk}$.

We illustrate this mismatch visually in Fig. 2, in which we can see the three lines with different slopes [Fig. 2(c)], each representing the phase of one soliton caused by the different temporal positions. Generally, these lines cannot intersect at the same point and a mismatch will occur when using the averaged position $\bar{\tau}$ as the mutual temporal offset for both the signal envelope and the sinusoidal fringes beneath it. Although this mismatch has a trivial effect upon the envelope profile given sufficient temporal stretching, it can have a nontrivial effect upon the fast-oscillating fringes beneath the envelope, which is sensitive to the phase difference. In practice, the relative phases between the solitons are usually retrieved using numerical fitting of the TS-DFT signal, while there is no prior temporal origin for the TS-DFT signal in the coordinate. The temporal origin of the TS-DFT signal envelope [$\bar{\tau}$ in Eq. (15)] is usually obtained out of the numerical fitting in which the temporal origin $\bar{\tau}$ is also set as a variable to be fitted (see Sec. III A). Nevertheless, a single temporal origin of the envelope cannot simultaneously coincide with the temporal origin of all the sinusoidal fringes. As a consequence, when we use the genuine interferogram profile given by Eq. (13) to retrieve the structure, there would be deterministic discrepancies in the relative phases. We can evaluate these particular discrepancies by rewriting Eq. (17) as

$$\Phi_j - \Phi_k = -\Delta\tau_{jk} \frac{\tau - \bar{\tau}}{\zeta} - (\Delta\varphi_{jk} + \Delta\varphi'_{jk}), \quad (21)$$

where $\Delta\varphi_{jk}$ is the actual carrier-phase difference between two solitons and $\Delta\varphi'_{jk}$ is the phase discrepancy caused by the mismatched offsets, which can be expressed as

$$\Delta\varphi'_{jk} = \Delta\tau_{jk} \frac{\bar{\tau} - \bar{\tau}_{jk}}{\zeta}. \quad (22)$$

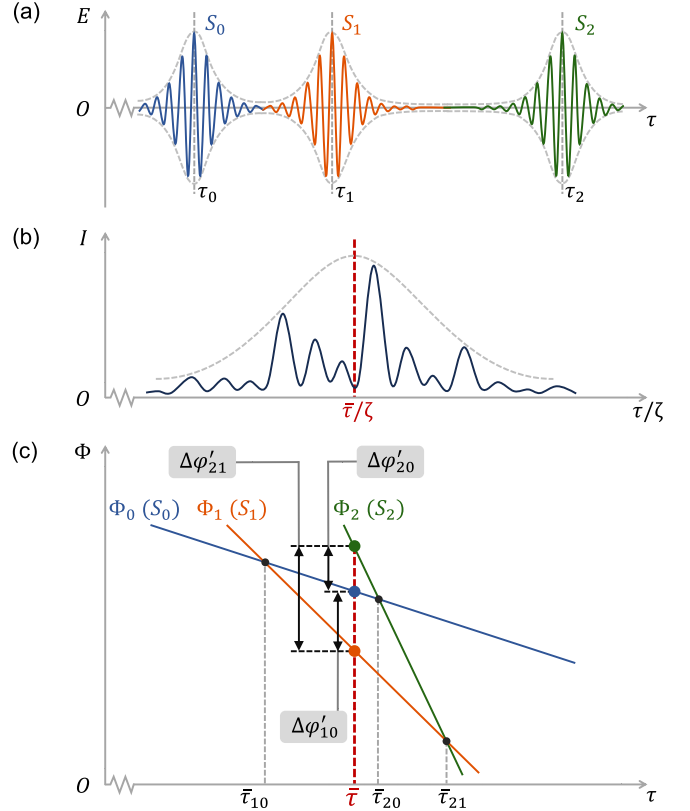


FIG. 2. Triple-soliton TS-DFT signal schematic. (a) A triple-soliton structure in the normalized time coordinate, with the three solitons denoted as S_0 , S_1 , and S_2 and their temporal positions at τ_0 , τ_1 , and τ_2 . (b) The triple-soliton TS-DFT signal (blue curve) with envelope plotted as a gray dashed line in the mapped-frequency (τ/ζ) coordinate. $\bar{\tau}$ is the center of the entire envelope. (c) The linear term of Φ for the three solitons [second term in Eq. (9)] depicted as three lines that pairwise intersect at $\bar{\tau}_{jk}$. Their differences at $\bar{\tau}$ are the phase mismatches $\Delta\varphi'_{jk}$ in Eq. (22).

Equation (22) is an intrinsic consequence of the unmatched mapping relations given in Eqs. (19) and (20). We can notice that this discrepancy depends both on the mismatch in the averaged positions, $\bar{\tau} - \bar{\tau}_{jk}$, and on the soliton spacing $\Delta\tau_{jk}$ which serves as a magnification coefficient. Therefore, the retrieved relative phase is actually mixed-up information of both the phase and position relations. Equation (22) also suggests that when the dispersion broadening is insufficient (i.e., a small ζ with respect to the soliton spacing $\Delta\tau_{jk}$), the phase discrepancy also becomes obvious.

From the preceding analysis, we can realize that the TS-DFT signal of a double-soliton structure is only a special case in which a linear relationship between the TS-DFT signal and the spectral interferogram can be reestablished by a simple shift of the temporal origin [Eq. (12)]. For triple-soliton structures, the mismatch cannot be fixed in the same way since the averaged position of each pair of solitons has a different offset with the averaged position for all solitons (e.g., the position of the overall envelope). Such mismatch also exists for structures with more solitons, as we can readily expect. In these structures, the mismatch will be particularly prominent for adjacent solitons at the edge of the structures which has the

largest mismatch with the averaged position with the overall structure. The underlying source of such mismatch is actually the quadratic phase term in Eq. (3) induced by the dispersive stretching. When dealing with a multipulse profile, this quadratic phase term distorts the linear temporal mapping of the TS-DFT signal by assigning a different temporal offset for each sinusoidal fringe (for each pair of solitons) beneath the stretched envelope. Therefore, relative phase mismatch occurs when fitting the multisoliton TS-DFT signal with the form of spectral interferogram, and this mismatch depends on the relative positions of all the pulses.

Remarkably, we can also reveal that the phase mismatch discussed above carries the symmetry information of the multisoliton structure. In fact, the spectral interferogram of a triple-soliton structure and its mirrored structure are identical, leading to inevitable ambiguities in structure retrieval (i.e., swapping $\Delta\tau_{10}$ and $\Delta\tau_{21}$, as well as $\Delta\varphi_{01}$ and $\Delta\varphi_{12}$, leads to the same spectral interferogram). The phase discrepancy caused by the quadratic phase term [Eq. (22)], however, has opposite sign for mirrored structures, which therefore can be regarded as an “indicator” left by the structure that distinguishes itself from its mirrored structure.

III. NUMERICAL ANALYSIS

A. Relative phase discrepancies based on TS-DFT for triple-soliton structures

In practice, the TS-DFT signal obtained from multisoliton dynamics can be fit numerically using their spectral interferogram profiles so as to simultaneously retrieve the soliton spacing and relative phase. However, we have shown in the preceding section that the TS-DFT signal of a multisoliton structure is not a direct mapping of its spectral interferogram when given more than two solitons in the structure, which can lead to discrepancies in the relative phases. To demonstrate the typical magnitudes of such discrepancies from direct numerical fitting, we use a numerical example of a triple-soliton structure and compare the actual structure parameters with those retrieved from the TS-DFT signal.

The exemplary triple-soliton structure that we employed was set to have individual soliton positions at $\tau_0 = 0$, $\tau_1 = 10$, and $\tau_2 = 30$ (temporal positions normalized to the duration of an individual soliton), each with a carrier phase of $\varphi_0 = 0$, $\varphi_1 = 4\pi/3$, and $\varphi_2 = 2\pi/3$, respectively. The normalized TS-DFT signals of this particular triple-soliton structure at $\zeta = 50, 200$, and 500 (propagation distance normalized to dispersion length, which is approximately the temporal stretching ratio) are plotted in Fig. 3 using the time-frequency mapping relation given in Eq. (19), together with the genuine spectral interferogram. Here, both the spectral interferogram and the TS-DFT signal are normalized in terms of their envelope strength for easier comparison of their profiles. We can notice that the TS-DFT signal has a significant difference from the spectral interferogram when $\zeta = 50$ due to the phase discrepancies predicted above [see Fig. 3(a)]. Such discrepancies can be mitigated with much larger stretching ratios, as we can see in Figs. 3(b) and 3(c), where ζ has been increased to 200 and 500. However, even with an excessive stretching ratio [e.g., with $\zeta = 500$ in Fig. 3(c)], the TS-DFT signal still

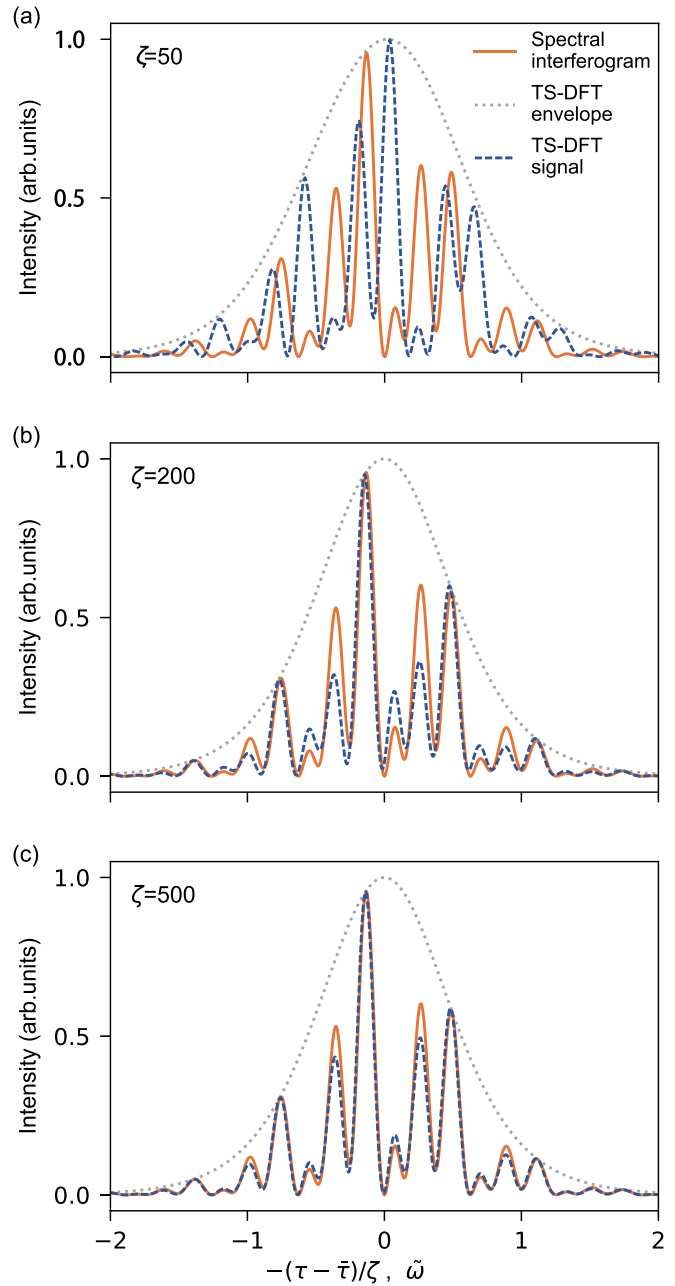


FIG. 3. The spectral interferogram (solid orange curves) and TS-DFT signals (dashed blue lines) of the triple-soliton structure under different ζ : (a) $\zeta = 50$, (b) 200, and (c) 500. The dashed gray curve gives the envelope of the TS-DFT signal. These curves are plotted in the normalized frequency coordinate [with the time-frequency mapping relation given by Eq. (19)].

exhibits some obvious discrepancies from the spectral interferogram in terms of detailed fringe structures, indicating that the TS-DFT signal for a triple-soliton structure is intrinsically not a linear mapping of the spectral interferogram, as we have analytically predicted above.

We then evaluate the consequent discrepancies in the retrieved structures using the TS-DFT signal and compare the results with our theoretical predictions given in Eq. (22). To retrieve the soliton spacings and relative phases from the TS-DFT signal, we employ the differential evolution (DE)

algorithm to perform the numerical fitting, which is simple and effective for solving the global optimal solution problem in continuous space [27,28]. The soliton spacing alone can also be retrieved based on the Wiener-Khinchin theorem [29], i.e., by taking the Fourier transform of the TS-DFT signal to obtain the autocorrelation function. Although the temporal resolution of this method is limited, we can use this approach to locate the optimal parameters faster during the numerical fitting. The fitting function based on the genuine profile of the spectral interferogram can be written as

$$F_{\text{fit}}(\zeta, \tau) = A \text{sech}^2 \left[\frac{\pi}{2\zeta} (\tau - \bar{\tau}) \right] \times \left\{ 3 + 2 \sum_{j=0}^2 \sum_{k=0}^{j-1} \cos \left[\frac{\Delta\tau_{jk}}{\zeta} (\tau - \bar{\tau}) - \Delta\varphi_{jk} \right] \right\}, \quad (23)$$

in which A represents the amplitude of the signal envelope, which equals unity for the normalized profile, and $\Delta\tau_{jk} = \tau_j - \tau_k$ and $\Delta\varphi_{jk} = \varphi_j - \varphi_k$, which are the spacing and the relative phase between the solitons located at τ_j and τ_k with carrier phases φ_j and φ_k . $\bar{\tau}$ represents the temporal offset of the signal envelope. In Fig. 3, we have neutralized this offset using $\bar{\tau}$ to facilitate the comparison with the spectral interferogram. The normalized propagation length ζ was set to vary from 50 to 500. The optimal fitting parameters for the spacings and relative phases after different propagation lengths are plotted in Fig. 4. We can first notice from Fig. 4(a) that the soliton spacings have been retrieved with high accuracy, even with very limited propagation lengths ($\zeta = 50$). The retrieved relative phases, on the contrary, have prominent discrepancies from the preset parameters (dashed lines), as plotted in Fig. 4(b), which could reach $\pi/2$ at $\zeta = 50$ and only gradually decrease to $\sim 0.1\pi$ when ζ reaches 500. We can then realize that the deviation of the TS-DFT signal from the spectral interferogram in Fig. 3(b) is dominantly caused by the phase discrepancy, while the retrieved spacings are largely decoupled from the relative phases.

As predict by Eq. (22), the discrepancies in the relative phases are deterministic, given a certain triple-soliton structure. Using the foreknown positions of each individual soliton in our numerical example, the predicted relative phases (i.e., $\Delta\varphi_{jk} + \Delta\varphi'_{jk}$), which are combinations of the actual relative phases and the position-dependent discrepancies, are plot in Fig. 4(b) (solid line), which agree quite well with the numerically retrieved results (solid diamonds). Therefore, we can confirm that the mismatch in the quadratic phase term (thus in the temporal origins for the envelope and the sinusoidal fringes) is the real source of the relative phase discrepancy, as we have predicted analytically.

B. Possible means to remove the relative phase discrepancies

Since the relative phase discrepancy in the multisoliton TS-DFT signal stems from the mismatch of quadratic phase terms induced by dispersive stretching, we can, in principle, remove it by compensating the quadratic phase term before the dispersive stretching. This can be achieved by using a radio-frequency phase modulator that adds a temporal phase

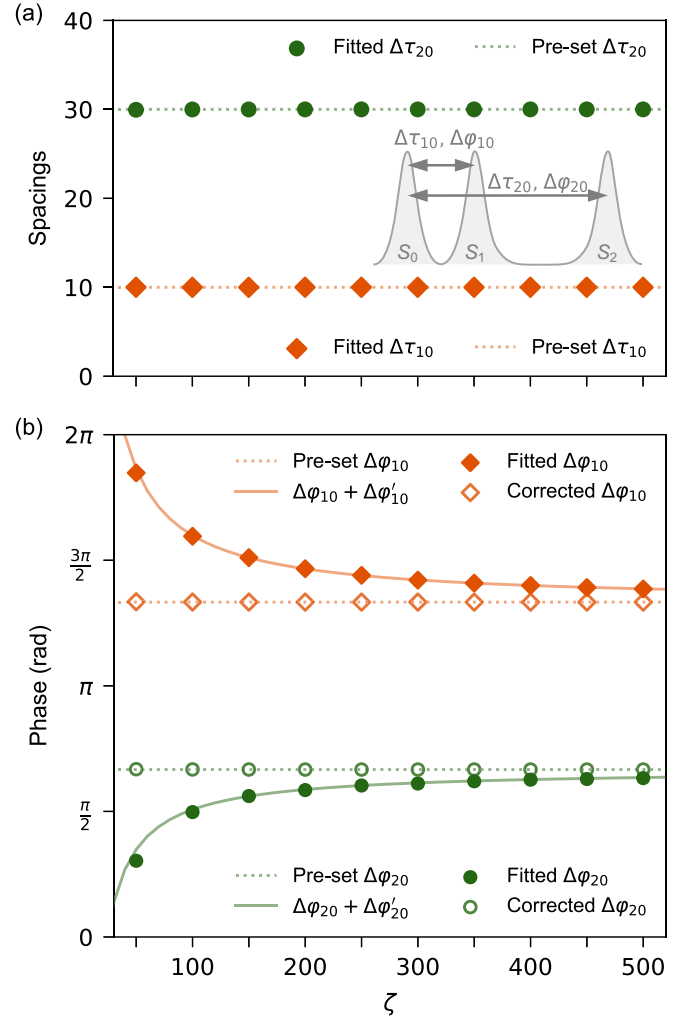


FIG. 4. (a) Fitted spacings and (b) fitted relative phases of the triple-soliton TS-DFT signal under different ζ (from 50 to 500). We use S_0 as the reference and consider its spacing and relative phases with the other two solitons. To indicate the corresponding results for the two pairs of solitons, we use orange diamond-dots for the results between S_0 and S_1 , while using green circular-dots for the results between S_0 and S_2 . The dotted lines represent the preset values of spacing and relative phases. The solid curves in (b) represent the relative phases with the intrinsic discrepancies [$\Delta\varphi_{j0} + \Delta\varphi'_{j0}$ in Eq. (21)], which well predicts the fitted relative phases based on Eq. (23). The hollow diamonds and dots represent the corrected fitting results using Eq. (25), which agree well with the preset values.

profile upon the multisoliton structure, which exactly cancels out the quadratic phase term [i.e., $\exp[-i\text{sgn}(\beta_2)\tau^2/2\zeta]$ in Eq. (3)], turning the TS-DFT signal of the individual solitons from Eq. (3) into

$$U(\zeta, \tau) = \frac{\tilde{U}[0, \text{sgn}(\beta_2) \frac{\tau}{\zeta}]}{[1 - i\text{sgn}(\beta_2)]\sqrt{\pi\zeta}}. \quad (24)$$

In this way, the resultant TS-DFT signal will be a complete linear mapping of the spectral interferogram despite having more than two solitons in the structure. The compensating phase profile depends on the duration of the individual solitons, the group velocity dispersion (GVD), and the length

of the dispersive fiber, which need to be known beforehand. Actually, analogies can be found in spatial Fraunhofer diffraction, where the far-field diffraction pattern also has a quadratic spatial-phase term. By using a lens with a proper focal length, we can remove this spatial-phase term, which results in the spatial Fourier transformation by the Fresnel diffraction [30,31].

The relative phase discrepancy can also be removed based on the fact that the sign of the discrepancy is related to the sign of the GVD of the dispersive fiber, as we can infer from Eq. (22). Therefore, if we use two pieces of dispersive fibers that can produce the same absolute value of group delay with opposite sign, the discrepancy can be simply canceled out by averaging the retrieved values.

At last, we also found that if we use a fitting function that allows for a different temporal shift for each sinusoidal fringe together with its own envelope in the TS-DFT signal, as given in Eq. (20), we can also retrieve the correct values for the relative phases. The general fitting function for an N -soliton structure can be written as

$$F_{\text{fit}}(\zeta, \tau) = A \sum_{j=0}^{N-1} \sum_{k=0}^{j-1} \text{sech}^2 \left[\frac{\pi}{2\zeta} (\tau - \bar{\tau}_{jk}) \right] \times \left\{ 2 + 2\cos \left[\frac{\Delta\tau_{jk}}{\zeta} (\tau - \bar{\tau}_{jk}) - \Delta\phi_{jk} \right] \right\}, \quad (25)$$

where we assign an independent offset $\bar{\tau}_{jk}$ for each pair of solitons in the structure that generates its own sinusoidal fringe. We used this fitting function to retrieve parameters from the same triple-soliton TS-DFT signal as analyzed in Sec. III A. Although the numerical fitting process was found to be slowed down significantly due to the more complicated fitting process, the retrieved values actually agree very well with the preset values, as we can see in Fig. 4(b) (hollow diamonds); meanwhile, no additional measurements or modulations of the TS-DFT signal are required.

IV. DISCUSSIONS

In reality, the retrieval of multisoliton structures using the TS-DFT method can be affected by a series of practical limitations beyond the intrinsic quadratic phase mismatch, as discussed in the preceding sections. For example, the fast electronics used for recording the TS-DFT signal may have a limited detection bandwidth and signal-to-noise ratio, which can distort the interferometric fringes given large soliton spacing or insufficient broadening, leading to discrepancies in the retrieved values. The higher-order dispersion of the dispersive fiber can become prominent when the optical bandwidth of the soliton is relatively large, which can lead to a time-warp effect [14] that causes nonlinear distortion of the TS-DFT signal and thus potential discrepancies in retrieving the structures. The multisoliton structure may also contain nonidentical solitons (e.g., with different amplitude or bandwidth) or even nonsoliton components (e.g., dispersive waves), which may cause

a blurred TS-DFT signal (with lower fringe contrast) that cannot be simply retrieved based on the simple assumptions as before. In light of all these practical limitations that require further investigations, this work pointed out that even if all of these limitations have been relieved, e.g., with improved equipment, there still exists an intrinsic discrepancy in the relative phases as a result of the dispersive propagation, which is irrelevant to any particular experimental setup.

We also noticed an important fact from the numerical results above that in general, the soliton spacing can always be retrieved with very high accuracy using the TS-DFT method. This high accuracy is maintained even with a very limited temporal stretching ratio, which is likely to occur in practice when we would like to avoid overlapping between consecutive shots given a high repetition rate, or to keep an adequate signal-to-noise ratio given low pulse energy. In contrast, the relative phase can have significant discrepancy using the same retrieval methods. We expect that the same conclusion may also hold with the influences from the various practical limitations. Therefore, precise measurements of the relative phases between the optical solitons probably demand further improvement for the original TS-DFT method.

V. CONCLUSIONS

In conclusion, we have analytically inferred that the TS-DFT signal of a multisoliton structure is not directly a linear mapping of their spectral interferogram given more than two solitons in the structure, which can lead to discrepancies when we retrieve the relative phases between the solitons. The underlying cause of this discrepancy is actually the mismatch of the quadratic phase term induced by the dispersive stretching for each soliton, in analogy with the spatial Fraunhofer diffraction, which leads to a different temporal offset for the sinusoidal fringe generated by each pair of solitons within the complicated TS-DFT signal. The discrepancy in the retrieved values of the relative phases has been predicted analytically and illustrated using numerical examples, which can be significant given a limited stretching ratio. We also proposed a means that can help to compensate for this discrepancy using improved measurements and numerical fitting methods. This work provides a theoretical prediction to the intrinsic discrepancy of the TS-DFT method used for resolving multisoliton structures, which can help to gain clearer insight of multisoliton dynamics in ultrafast lasers as well as other nonlinear optical systems.

ACKNOWLEDGMENTS

This work was supported by the National Natural Science Foundation of China (Grant No. 62375275), the Strategic Priority Research Program of the Chinese Academy of Sciences (Grant No. XDB0650000), the National Natural Science Foundation of China (Grant No. 62275254), Shanghai Science and Technology Plan Project Funding (Grant No. 23JC140100), the National High-level Talent Youth Project, and the Fuyang High-Level Talent Group Project.

[1] N. J. Zabusky and M. D. Kruskal, *Phys. Rev. Lett.* **15**, 240 (1965).

[2] G. Herink, F. Kurtz, B. Jalali, D. R. Solli, and C. Ropers, *Science* **356**, 50 (2017).

- [3] K. Krupa, K. Nithyanandan, U. Andral, P. Tchofo-Dinda, and P. Grelu, *Phys. Rev. Lett.* **118**, 243901 (2017).
- [4] J. Peng and H. Zeng, *Laser Photon. Rev.* **12**, 1800009 (2018).
- [5] Y. Liu, S. Huang, Z. Li, H. Liu, Y. Sun, R. Xia, L. Yan, Y. Luo, H. Liu, G. Xu, Q. Sun, X. Tang, and P. P. Shum, *Light Sci. Appl.* **12**, 123 (2023).
- [6] P. Grelu and N. Akhmediev, *Nat. Photon.* **6**, 84 (2012).
- [7] Y. Song, D. Zou, O. Gat, M. Hu, and P. Grelu, *Laser Photon. Rev.* **17**, 2300066 (2023).
- [8] Y. Zhou, Y.-X. Ren, J. Shi, H. Mao, and K. K. Y. Wong, *Optica* **7**, 965 (2020).
- [9] D. Y. Tang, W. S. Man, H. Y. Tam, and P. D. Drummond, *Phys. Rev. A* **64**, 033814 (2001).
- [10] A. Hause, H. Hartwig, M. Böhm, and F. Mitschke, *Phys. Rev. A* **78**, 063817 (2008).
- [11] L. Nimmegern, C. Beckh, H. Kempf, A. Leitenstorfer, and G. Herink, *Optica* **8**, 1334 (2021).
- [12] S. Liu, Y. Cui, E. Karimi, and B. A. Malomed, *Optica* **9**, 240 (2022).
- [13] D. R. Solli, J. Chou, and B. Jalali, *Nat. Photon.* **2**, 48 (2008).
- [14] K. Goda and B. Jalali, *Nat. Photon.* **7**, 102 (2013).
- [15] A. Mahjoubfar, D. V. Churkin, S. Barland, N. Broderick, S. K. Turitsyn, and B. Jalali, *Nat. Photon.* **11**, 341 (2017).
- [16] W. He, M. Pang, D.-H. Yeh, J. Huang, and P. S. J. Russell, *Light Sci. Appl.* **10**, 120 (2021).
- [17] J. Igbonacho, K. Nithyanandan, K. Krupa, P. T. Dinda, P. Grelu, and A. B. Moubissi, *Phys. Rev. A* **99**, 063824 (2019).
- [18] Y. Luo, R. Xia, P. P. Shum, W. Ni, Y. Liu, H. Q. Lam, Q. Sun, X. Tang, and L. Zhao, *Photon. Res.* **8**, 884 (2020).
- [19] Y. Guo, W. Lin, W. Wang, R. Zhang, T. Liu, Y. Xu, X. Wei, and Z. Yang, *Nat. Commun.* **14**, 2029 (2023).
- [20] X. Hu, J. Guo, J. Wang, J. Ma, L. Zhao, S. Yoo, and D. Tang, *Light Sci. Appl.* **12**, 38 (2023).
- [21] Z. Q. Wang, K. Nithyanandan, A. Coillet, P. Tchofo-Dinda, and P. Grelu, *Nat. Commun.* **10**, 830 (2019).
- [22] S. Hamdi, A. Coillet, B. Cluzel, P. Grelu, and P. Colman, *Phys. Rev. Lett.* **128**, 213902 (2022).
- [23] J. He, M. Zhou, C. Liu, P. Wang, D. Xing, J. Li, Y. Liu, and Z. Wang, *Opt. Express* **31**, 22776 (2023).
- [24] W. He, M. Pang, D. H. Yeh, J. Huang, C. R. Menyuk, and P. S. J. Russell, *Nat. Commun.* **10**, 5756 (2019).
- [25] A. V. Andrianov, *IEEE Photon. Technol. Lett.* **34**, 39 (2022).
- [26] K. Goda, D. R. Solli, K. K. Tsia, and B. Jalali, *Phys. Rev. A* **80**, 043821 (2009).
- [27] S. Das and P. N. Suganthan, *IEEE Trans. Evol. Computat.* **15**, 4 (2011).
- [28] R. Storn and K. Price, *J. Glob. Optim.* **11**, 341 (1997).
- [29] L. Cohen, *IEEE Signal Process. Lett.* **5**, 292 (1998).
- [30] B. H. Kolner and M. Nazarathy, *Opt. Lett.* **14**, 630 (1989).
- [31] C. V. Bennett and B. H. Kolner, *IEEE J. Quantum Electron.* **36**, 430 (2000).